THE JOURNAL OF PHYSICAL CHEMISTRY Letters

Letter

Computational Characterization of Defects in Metal-Organic Frameworks: Spontaneous and Water-Induced Point Defects in ZIF-8

Chenyang Zhang, Chu Han, David S. Sholl, and Jordan R. Schmidt

J. Phys. Chem. Lett., **Just Accepted Manuscript** • DOI: 10.1021/acs.jpclett.5b02683 • Publication Date (Web): 15 Jan 2016

ACS Publications

The Journal of Physical Chemistry Letters is published by the American Chemical Society. 1155 Sixteenth Street N.W., Washington, DC 20036

Computational Characterization of Defects in Metal-Organic Frameworks: Spontaneous and Water-induced Point Defects in ZIF-8

Chenyang Zhang[1], Chu Han[2], David S. Sholl[3], and J. R. Schmidt[1]*

[1]Theoretical Chemistry Institute and Department of Chemistry, University of Wisconsin-Madison, 1101 University Ave, Madison, Wisconsin 53706, United States.

[2]School of Chemistry & Biochemistry, Georgia Institute of Technology, Atlanta, Georgia 30332, United States

[3]School of Chemical & Biomolecular Engineering, Georgia Institute of Technology, 311 Ferst Drive NW, Atlanta, Georgia 30332-0100, United States.

Corresponding Author

*Email: schmidt@chem.wisc.edu

ABSTRACT

Zeolitic imidazole frameworks (ZIFs) are an important class of porous crystalline metal-organic framework (MOF) materials that have attracted widespread attention for applications ranging from gas adsorption and separation to catalysis. Although the bulk crystal structures of MOFs are typically well characterized, comparatively little is known regarding MOF defect structures. Drawing on analogies with conventional silicon-based zeolites, we utilize computational

methods to examine the structure and stability of putative point-defect structures (including vacancies, substitutions, and "dangling" linkers) within the prototypical ZIF-8 structure. Considering both post-synthetic (gas-phase) and synthetic (solution-phase) conditions, we find that several of the defect structures lie low in energy relative to the defect-free parent crystal, with barriers to defect formation that are large but surmountable under relevant temperatures. These results are consistent with prior experimental observations of ZIF stability and reactivity and suggest that defects may play an important role in influencing the long-term stability of MOFs under conditions that include exposure to water vapor and trace contaminants such as acid gases.

TOC GRAPHIC

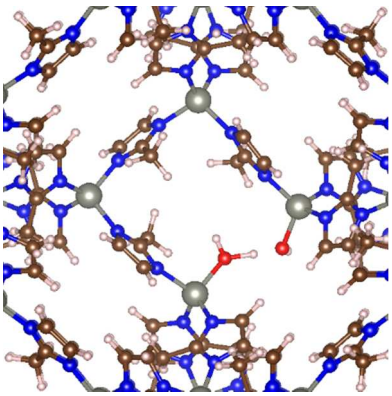

KEYWORDS zeolitic imidazolate framework, vacancy, substitution, density functional theory

Metal organic frameworks (MOFs) are nano-porous crystalline materials composed of metal cations coordinated by bridging organic linkers.[1] Within the large family of MOFs, zeolitic imidazolate frameworks (ZIFs), composed of tetrahedrally coordinated zinc or cobalt cations and bridging imidazolate (Im) ligands, have received special attention due to their unusual stability,

structural and chemical diversity, and their promising applications including sensing[2], storage and separation of gases[3–11] drug delivery[12,13] and catalysis[14]. The bulk structure of ZIFs and other MOFs are typically well understood on the basis of x-ray diffraction (XRD) experiments, and large collections of crystal structures are now available.[15] In the specific case of ZIFs, the similarity of the Zn-Im-Zn bond angle to the Si-O-Si angle in conventional silicon-based zeolites gives rise to topologically similar crystal structures. Yet in contrast to zeolites,[16–20] whose defect structures are well known and well characterized, comparatively little is known with regard to the structure and stability of elementary point defect structures (e.g. metal / ligand vacancy, dangling linkers) within ZIFs and other MOF crystals,[21] and direct experimental evidence for such defects (especially in stable, low-connected MOFs such as ZIFs) is sparse. Nonetheless, such defects likely play an important role in influencing the physical properties, reactivity[22–28] and long-term stability[21,29,30] of MOFs.

Motivated by similarities with traditional zeolites, in this Letter we computationally examine the thermodynamic stability and kinetic accessibility of various point defects in ZIFs. We assess the thermodynamic stability of each defect by calculating the energy change of a putative defect formation reaction, under both synthetic (solution-phase) and post-synthetic (gas-phase) conditions. By analogy with defects known to exist in zeolites, we examine both metal / linker vacancies, as well as potential "dangling" linker groups (see **Figure 1**).[21,31–33] We also study the kinetic feasibility of defect formation and discuss the implications of our results in terms of the reactivity and long-term stability of MOFs under working conditions that may involve exposure to water vapor or acid gases[34].

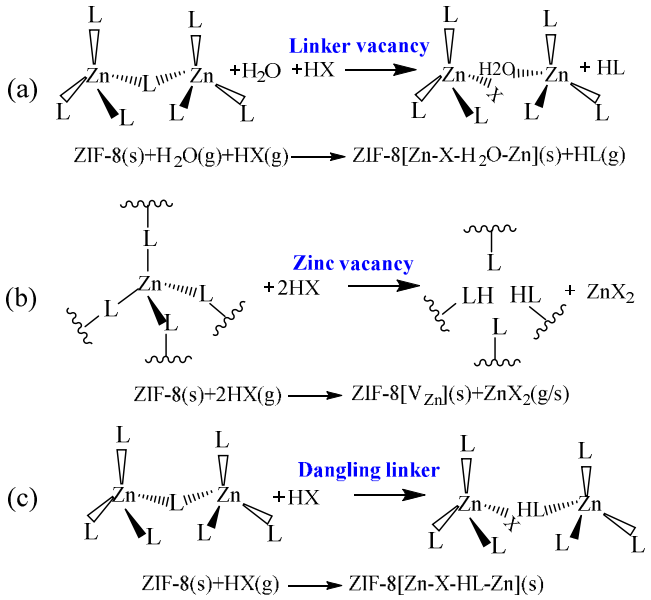

Figure 1. *Schematic illustration of various potential ZIF point defects and associated formation reactions: (a) Linker vacancy, (b) Zinc vacancy and (c) Dangling linker. X = OH^-, NO_3^- or $COOH^-$. Zn-X-H_2O-Zn, V_{Zn}, Zn-X-HL-Zn denotes a linker vacancy, zinc vacancy, and dangling linker, respectively.*

We utilize ZIF-8 as prototypical model ZIF. ZIF-8 is composed of zinc(II) cations coordinated by 2-methylimidzaolate ligands and forms a porous crystalline solids with sodalite topology.[35] Although our calculations focus on ZIF-8, we expect our qualitative conclusions to be transferable to other ZIFs, which differ only in the functionalization of the organic linker but otherwise maintain identical local structure. For each putative defect formation reaction, we use density functional theory (DFT) calculations to estimate the associated energy change relative to the bulk, defect-free structure, either under synthetic or post-synthetic conditions. These scenarios are distinguished by the presence or absence of solvent, typically (in the case of ZIFs) DMF[35], methanol[36], or water[37]. We include such solvation effects using a combination of experimentally measured or computationally estimated aqueous solvation enthalpies. Within

these defect formation reactions, we include the possibility of reactions involving water (either ambient or residual solvent), NO_3^- (a typical counterion during synthesis) or formate (a modulator often used in ZIF synthesis)[38,39]. Since our goal is to examine the plausibility of various defects (rather than to estimate absolute defect concentrations), we neglect entropic effects, the inclusion of which is both challenging (due to the anharmonicity of low-frequency phonons and the uncertainty in solution-phase translation/rotational entropy) and unlikely to qualitatively alter our conclusions (see Supporting Information, Table S5). Additional details can be found in the Computational Methods and Supporting Information.

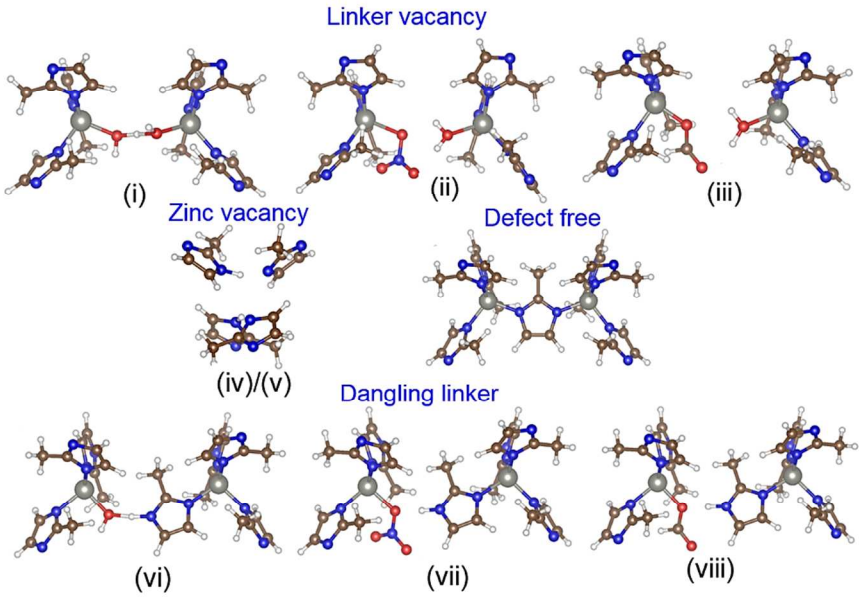

Figure 2. *Local structures of the defects in ZIF-8 (numbering corresponds to the defect formation reactions in Table 1). Linker vacancies (i)-(iii), zinc vacancies (iv-v) and dangling linkers (vi-viii). The local structure of defect-free ZIF-8 is shown for comparison. H, C, N, O and Zn are shown in white, brown, blue, red and gray, respectively. Reactions (iv)/(v) yield identical point defect structure.*

Calculated zero-point corrected gas-phase (ΔE^{gas}) and solution-phase (ΔE^{soln}) defect formation energies are shown in **Table 1**. Similar to an oxygen vacancy in zeolites, a linker vacancy can be formed by removing a neutral, protonated imidazole linker (to the gas-phase or bulk solution) via reaction with a water and an additional proton donating group (**Figure 1**a, reactions (i)-(iii) of**Table 1**). Within the context of this simple description, the resulting two unsaturated metal sites are then filled by an associating water and the conjugate base of the proton donating group. The local optimized structure of the resulting defect is shown in **Figure 2**, with gas-phase defect formation energies ranging between 14.5 and -0.5 kcal/mol, depending on the nature of the proton donating group. Note that these energies are calculated with respect to non-interacting reactants and products; as such, a significant energetic contribution comes from desorption of the resulting gas-phase imidazole from the ZIF. Since it is likely that the imidazole would remain adsorbed within the ZIF, we also calculate energies relative to the interacting products (e.g. adsorbed imidazole), yielding smaller formation energies between -3.6 and -8.0 kcal/mol (numbers in parentheses in **Table 1** and Figure S3). Including solvation effects for the reactants and products, we estimate the corresponding aqueous solution-phase linker vacancy formation energies to be slightly more favorable, between 10.6 and -3.8 kcal/mol (-7.5 to -11.3 for adsorbed imidazole). Crucially, irrespective of the details of the proposed formation, many of the resulting formation energies are approximately thermoneutral or even exothermic, suggesting the thermodynamic plausibility of linker vacancy point defects under ambient conditions. Of course formation of such a linker vacancy requires cleavage of two strong metal-ligand dative bonds and thus likely presents significant kinetic barriers (vide infra).

We also consider the possibility of forming a metal cation vacancy, analogous with well-known tetrahedral vacancies in zeolites (**Figure 1**b, reactions (iv)-(v) of **Table 1** and Figure S2

in the Supporting Information).[21,33] Within our model, two of the resulting unsaturated linkers are protonated by two proton-donating groups, with the zinc reacting with the resulting conjugate base. In the gas-phase, the mechanistically most feasible zinc-containing product is an ion-paired salt complex and the resulting defect formation energies range between about 20 and 50 kcal/mol due to the relative instability of the ion-pair (numbers given in brackets in). Alternatively, the defect energy can be calculated relative to solid (crystalline) salt products, yielding much smaller energies between -5.9 and -38.2 kcal/mol, although the formation of such a crystalline salt product within a gas-phase reaction seems mechanistically unlikely. The solution-phase metal vacancy formation energies were calculated assuming a (potentially partially) dissolved salt product, with energies of -25.0 kcal/mol (for $X = NO_3^-$) and 21.0 kcal/mol ($X = OH^-$), with the former driven both by stronger proton donating power and by solvation of the resulting (soluble) $Zn(NO_3)_2$ salt. Once again, based purely on the thermodynamics of the defect formation reactions (neglecting entropic factors), metal vacancy formation within ZIF-8 is thermodynamically plausible.

Table 1. *Formation energies of the possible point defects in ZIF-8. All energetics are calculated at the PBE-D3 level with values given in kcal/mol.* ΔE^{gas}, $\Delta\Delta E^{solv}$, *and* ΔE^{soln} *denote the gas-phase defect formation reaction energy (see Figure 1), solvation correction and resulting solution-phase formation energy. Numbers in square brackets correspond to gas-phase ion-paired* $Zn(OH)_2/Zn(NO_3)_2$ *products, which are shown alongside results assuming crystalline salt products. In the case of linker vacancies, energies in parentheses are taken with respect to interacting product complex; all other energies are with respect to non-interacting reactants and products.*

(kcal/mol)		Defect	ΔE^{gas}	$\Delta\Delta E^{solv}$	ΔE^{soln}
Linker vacancy	(i)	Zn-OH…H_2O-Zn	14.5(-3.6)	-3.9	10.6(-7.5)
	(ii)	Zn-NO_3… H_2O-Zn	3.8(-6.2)	-2.8	1.0(-9.0)
	(iii)	Zn-COOH…H_2O-Zn	-0.5(-8.0)	-3.3	-3.8(-11.3)
Zn vacancy	(iv)	$V_{Zn}[Zn(OH)_2]$	-5.9 [46.0]	26.9	21.0
	(v)	$V_{Zn}[Zn(NO_3)_2]$	-38.2[21.8]	13.2	-25.0
Dangling linker	(vi)	Zn-OH…HmIM-Zn	11.9	8.8	20.7
	(vii)	Zn-NO_3…HmIM-Zn	6.2	6.8	13.0
	(viii)	Zn-COOH…HmIM-Zn	2.9	0.5	3.4

The increased conformational flexibility and linker group size of ZIFs relative to zeolites offers the possibility for an additional defect type: a "dangling" linker group, where the "bridging" imidazolate linker is bound to one, rather than two, adjacent zinc cations. This defect can also be considered an intermediate in the pathway to a linker vacancy. Within our model, the dangling linker is generated via reaction of the ZIF with a single proton donating group (see Figure 1c, reactions (vi)-(viii) of Table 1, and Figure S2 in supporting information). Whether in the gas- or solution-phase, the resulting defect formation energies are typically higher, between

2.9-11.9 (gas-phase) and 3.4-20.7 (solution-phase) kcal/mol. Analysis of our DFT energies suggests that the increase in dangling linker formation energy relative to linker vacancies is driven by the strain / deformation of the ZIF lattice, which must accommodate the bulky dangling imidazolate linker within the confined ZIF pore. This strain energy might be reduced for ZIFs containing a larger pore diameter. The higher formation energy of dangling linkers versus linker vacancies suggests a decreased concentration of the former relative to the latter, and considering the dangling linker as an intermediate towards linker vacancy formation, also provides one possible explanation for the observed thermal and chemical kinetic stability of ZIFs.[4,6,35,40]

Our results also suggest a possible explanation for well-known post-synthetic linker[36,41–43] and metal[36] exchange processes in ZIFs. In such post-synthetic exchange processes, a ZIF is submerged in a concentrated solution of an alternative linker group or metal, where slow in situ replacement of the linker/metal via a single-crystal to single-crystal transformation is observed. In the case of ZIF-8 linker exchange, one example of such a process requires elevated temperatures (100°C) and extended reaction times (~6 days), resulting in ~85% replacement of the methyl-imidazolate by an unfunctionalized imidazolate and yielding a structure that cannot be accessed via direct synthesis.[42] We hypothesize that such single crystal transformations could be driven by the transient formation of point defects, including metal/linker vacancies, that are then quenched by replacement with an alternative linker / metal.[42] Recent experimental evidence suggests that these defects need not be merely transient. Cheng et al.[44] measured the XRD pattern of ZIF-8 exposed to liquid water and found evidence for several new XRD peaks that increased in intensity with exposure while the original diffraction peaks decreased. They also find IR evidence for water that cannot be desorbed even at 100°C. They interpret this data in

terms of water-terminated defect sites and find that these defects permanently increase the H_2 uptake of the material.

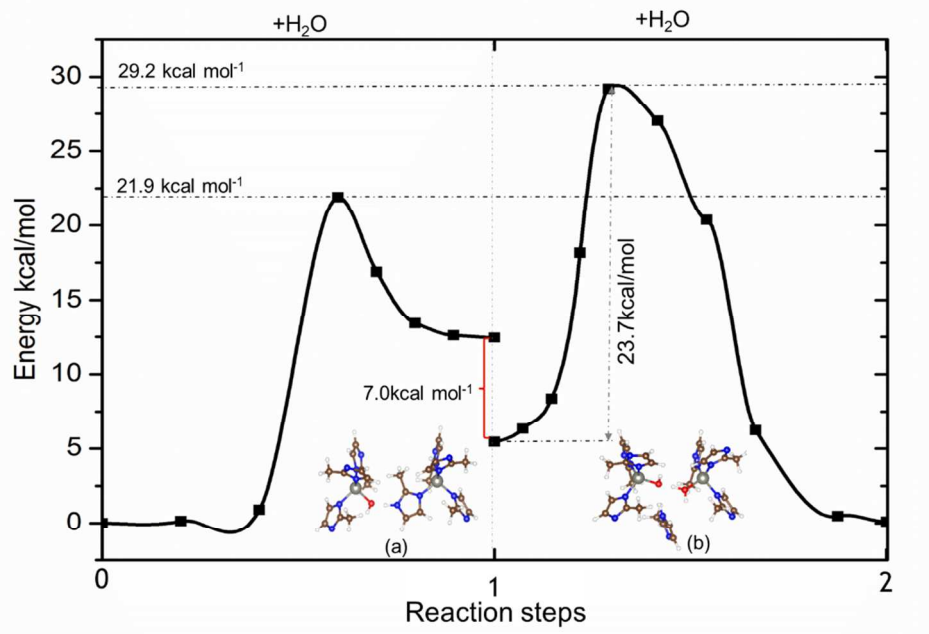

Figure 3. *Minimum energy reaction pathways for the linker vacancy formation via reaction with water (reaction (i) of Table 1). The reaction proceeds via two steps, first forming a dangling linker (1), and subsequently a linker vacancy (2). The energetic discontinuity between the two steps arises from the heat of adsorption of the 2nd water molecule.*

Insight regarding the kinetics of defect formation can be gained by examining the activation energy and minimum energy pathway associated with defect formation. This reaction pathway is shown for linker vacancy formation (reaction (i) of **Table 1**) in Figure 3. Starting with a defect-free ZIF, linker vacancy formation proceeds via reaction with water over a barrier of ~22 kcal/mol to form a meta-stable dangling linker intermediate. Reaction with a second water proceeds with a higher effective barrier of ~29 kcal/mol, leading to a relatively low-energy linker vacancy defect. Both barriers are estimated under gas-phase conditions and may be modified slightly by inclusion of solvent effects. The overall energetics presented here differ slightly from

the data in **Table 1**, since the latter energetics are taken with respect to non-interacting reactants/products. The calculated reaction barriers are sizable, reflecting the observed thermal and kinetic stability of ZIFs in aqueous solution. Nonetheless, crude transition state theory calculations ($k(T) = \frac{k_B T}{h} e^{-\Delta^{\ddagger} E/RT}$, neglecting all entropic effects) would predict the barrier to dangling linker formation to be surmountable at room temperature on a timescale of ~1 hour, consistent with recent observations of water-terminated defect sites (presumably dangling linkers) in ZIF-8 under ambient conditions.[44] The higher effective barrier to linker vacancy formation would be accessible only at higher temperatures, with transition state theory predicting timescales of ~5 hours at 100°C. In both cases, inclusion of solvation effects may slightly reduce the calculated barrier, while use of hybrid functionals may somewhat increase the barrier. Nonetheless, an effective barrier of this magnitude is qualitatively consistent with the experimental conditions required for linker exchange.

Overall, these results challenge the simplistic interpretation of ZIFs as perfect defect-free crystals. While we do not attempt to estimate absolute equilibrium defect concentrations (due to neglect of entropic effects, which are difficult to quantify, particularly in solution), it is clear that elementary linker and metal vacancy defects are relatively low in energy such that their presence should not be thermodynamically unexpected. However, our results also indicate that kinetic factors are likely to inhibit the introduction of large defect concentrations, at least at room temperature. Yet even very small spontaneous equilibrium defect concentrations may have a potentially outsized impact on the catalytic properties or long-term stability of ZIFs and other MOFs, particularly under "reactive" working conditions where the defect site may be exposed to reactants/solvents, trace contaminants, or acid gases. As such, these results also highlight the importance of considering the presence and impact of such defects when assessing the viability

of ZIFs and other "stable" MOFs for targeted applications. At the same time, our results should spur additional experimental studies to characterize MOF defects and their impacts.

Computational Methods

A periodic model of ZIF-8 was constructed from the XRD crystal structure obtained from the Cambridge Structural Database (CSD).[35] The cubic unit cell includes 276 atoms with a lattice constant of 16.991 Å. Periodic calculations utilized the Vienna Atomistic Simulation Package (VASP) in conjunction with a 600 eV energy cutoff and a projector-augmented wave (PAW) treatment of core electrons.[45–50] All structural optimizations utilized the PBE functional with the lattice constant fixed to that of the defect-free ZIF, and atoms were relaxed to a tolerance of 10^{-2} eV/Å. The use of the fixed, defect-free, lattice constant is motivated by the desire to study defect formation thermodynamics at the expected (low) concentration, where the ZIF lattice constant will be unaltered be dilute defects; due to periodic boundary conditions, relaxation of the lattice for defective structures this would be representative of unphysically high defect concentrations. All energy differences were subsequently evaluated using both dispersion corrected PBE-D3 (main text) and also the hybrid B3LYP-D3 functional (see Table S1 in Supporting Information); the energetics are qualitatively unchanged at the B3LYP-D3 level. The PBE geometries are used in all cases for consistency and efficiency, resulting in energy differences of < 1 kcal/mol with respect to full optimizations (see Tables S2-S3). Energy differences involving isolated molecules were evaluated by placing the molecule within a box with the same dimensions as the unit cell in order to generate a consistent periodic system (see Figure S2). Zero-point corrections were calculated and applied based on a normal mode analysis at the PBE level. Reaction pathway investigations were performed via the nudged elastic band (NEB) method on the full,

periodic, ZIF-8 unit cell using 8 images for each of the two reaction steps and then refined via climbing-image NEB.[51,52] The resulting images are approximately evenly distributed along the minimum energy pathway connecting reactants and products according to the NEB scheme.

Solution-phase energy differences were calculated by adding a solvation corrections to all reactants and products in each defect formation reaction (see Figure S4). Aqueous solvation energies for simple species (H_2O, HNO_3, HCOOH, $Zn(NO_3)_2$, $Zn(OH)_2$) were estimated using experimentally measured enthalpies of dissolution / condensation (see Table S4). For gaseous reagents, ideal gas behavior was assumed for conversions for enthalpies to energies. Aqueous solvation energies for the remaining species were estimated computationally using finite "cluster" models in conjunction with the SMD[53] polarizable continuum solvation model. These solvation energies were added to the (periodic) gas-phase reaction energetics to yield estimates for the corresponding solution-phase reactions. See Supporting Information for complete details.

ASSOCIATED CONTENT

Supporting Information

Additional computational details; B3LPY-D3 results; optimized lattice constants at the PBE and PBE-D3 levels; estimates of solvation effects for all reactants and products; estimates of entropic effects.

AUTHOR INFORMATION

Corresponding Author

*Email: schmidt@chem.wisc.edu

Notes: The authors declare no competing financial interests.

ACKNOWLEDGMENT

This work was financially supported by the Center for "Understanding and Control of Acid Gas-induced Evolution of Materials for Energy", an Energy Frontier Research Center funded by DOE, Office of Science, BES under Award #DESC0012577. Computational resources were provided in part by National Science Foundation Grant CHE-0840494 and using the compute resources and assistance of the UW-Madison Center for High Throughput Computing (CHTC) in the Department of Computer Sciences. The CHTC is supported by UW-Madison, the Advanced Computing Initiative, the Wisconsin Alumni Research Foundation, the Wisconsin Institutes for Discovery, and the National Science Foundation, and is an active member of the Open Science Grid, which is supported by the National Science Foundation and the U.S. Department of Energy's Office of Science. J.R.S is a Camille Dreyfus Teacher-Scholar.

REFERENCES

(1) Zhou, H.-C.; Long, J. R.; Yaghi, O. M. Introduction to Metal-Organic Frameworks. *Chem. Rev.* **2012**, *112*, 673–674.

(2) Ma, W.; Jiang, Q.; Yu, P.; Yang, L.; Mao, L. Zeolitic Imidazolate Framework-Based Electrochemical Biosensor for in Vivo Electrochemical Measurements. *Anal. Chem.* **2013**, *85*, 7550–7557.

(3) Bae, Y.-S.; Lee, C. Y.; Kim, K. C.; Farha, O. K.; Nickias, P.; Hupp, J. T.; Nguyen, S. T.; Snurr, R. Q. High Propene/propane Selectivity in Isostructural Metal-Organic Frameworks

with High Densities of Open Metal Sites. *Angew. Chem. Int. Ed. Engl.* **2012**, *51*, 1857–1860.

(4) Banerjee, R.; Phan, A.; Wang, B.; Knobler, C.; Furukawa, H.; O'Keeffe, M.; Yaghi, O. M. High-Throughput Synthesis of Zeolitic Imidazolate Frameworks and Application to CO2 Capture. *Science* **2008**, *319* , 939–943.

(5) Zhang, L.; Wu, G.; Jiang, J. Adsorption and Diffusion of CO2 and CH4 in Zeolitic Imidazolate Framework-8: Effect of Structural Flexibility. *J. Phys. Chem. C* **2014**, *118*, 8788–8794.

(6) Wang, B.; Côté, A. P.; Furukawa, H.; O'Keeffe, M.; Yaghi, O. M. Colossal Cages in Zeolitic Imidazolate Frameworks as Selective Carbon Dioxide Reservoirs. *Nature* **2008**, *453*, 207–211.

(7) Wu, H.; Zhou, W.; Yildirim, T. Hydrogen Storage in a Prototypical Zeolitic Imidazolate Framework-8. *J. Am. Chem. Soc.* **2007**, *129*, 5314–5315.

(8) Eum, K.; Jayachandrababu, K. C.; Rashidi, F.; Zhang, K.; Leisen, J.; Graham, S.; Lively, R. P.; Chance, R. R.; Sholl, D. S.; Jones, C. W.; et al. Highly Tunable Molecular Sieving and Adsorption Properties of Mixed-Linker Zeolitic Imidazolate Frameworks. *J. Am. Chem. Soc.* **2015**, *137* , 191–4197.

(9) Basnayake, S. A.; Su, J.; Zou, X.; Balkus, K. J. Carbonate-Based Zeolitic Imidazolate Framework for Highly Selective CO2 Capture. *Inorg. Chem.* **2015**, *54*, 1816–1821.

(10) Pimentel, B. R.; Parulkar, A.; Zhou, E.; Brunelli, N. A.; Lively, R. P. Zeolitic Imidazolate Frameworks: Next-Generation Materials for Energy-Efficient Gas Separations. *ChemSusChem* **2014**, *7*, 3202–3240.

(11) Yao, J.; Wang, H. Zeolitic Imidazolate Framework Composite Membranes and Thin Films: Synthesis and Applications. *Chem. Soc. Rev.* **2014**, *43*, 4470–4493.

(12) Zhuang, J.; Kuo, C.-H.; Chou, L.-Y.; Liu, D.-Y.; Weerapana, E.; Tsung, C.-K. Optimized Metal-Organic-Framework Nanospheres for Drug Delivery: Evaluation of Small-Molecule Encapsulation. *ACS Nano* **2014**, *8*, 2812–2819.

(13) Cai, W.; Chu, C.-C.; Liu, G.; Wáng, Y.-X. J. Metal-Organic Framework-Based Nanomedicine Platforms for Drug Delivery and Molecular Imaging. *Small* **2015**, *11*,

4806–4822.

(14) Fujita, M.; Kwon, Y. J.; Washizu, S.; Ogura, K. Preparation, Clathration Ability, and Catalysis of a Two-Dimensional Square Network Material Composed of Cadmium(II) and 4,4'-Bipyridine. *J. Am. Chem. Soc.* **1994**, *116*, 1151–1152.

(15) Chung, Y. G.; Camp, J.; Haranczyk, M.; Sikora, B. J.; Bury, W.; Krungleviciute, V.; Yildirim, T.; Farha, O. K.; Sholl, D. S.; Snurr, R. Q. Computation-Ready, Experimental Metal–Organic Frameworks: A Tool To Enable High-Throughput Screening of Nanoporous Crystals. *Chem. Mater.* **2014**, *26*, 6185–6192.

(16) Sokol, A. A.; Catlow, C. R. A.; Garcés, J. M.; Kuperman, A. Local States in Microporous Silica and Aluminum Silicate Materials. 1. Modeling Structure, Formation, and Transformation of Common Hydrogen Containing Defects. *J. Phys. Chem. B* **2002**, *106*, 6163–6177.

(17) Malola, S.; Svelle, S.; Bleken, F. L.; Swang, O. Detailed Reaction Paths for Zeolite Dealumination and Desilication From Density Functional Calculations. *Angew. Chemie Int. Ed.* **2012**, *51*, 652–655.

(18) Fjermestad, T.; Svelle, S.; Swang, O. Mechanism of Si Island Formation in SAPO-34. *J. Phys. Chem. C* **2015**, *119*, 2086–2095.

(19) Fjermestad, T.; Svelle, S.; Swang, O. Desilication of SAPO-34: Reaction Mechanisms from Periodic DFT Calculations. *J. Phys. Chem. C* **2015**, *119*, 2073–2085.

(20) Pascale, F.; Ugliengo, P.; Civalleri, B.; Orlando, R.; D'Arco, P.; Dovesi, R. Hydrogarnet Defect in Chabazite and Sodalite Zeolites: A Periodic Hartree–Fock and B3-LYP Study. *J. Chem. Phys.* **2002**, *117*, 5337.

(21) Sholl, D. S.; Lively, R. P. Defects in Metal–Organic Frameworks: Challenge or Opportunity? *J. Phys. Chem. Lett.* **2015**, *6*, 3437–3444.

(22) Fang, Z.; Bueken, B.; De Vos, D. E.; Fischer, R. A. Defect-Engineered Metal-Organic Frameworks. *Angew. Chem. Int. Ed. Engl.* **2015**, *54*, 7234–7254.

(23) Furukawa, H.; Müller, U.; Yaghi, O. M. "Heterogeneity within Order" in Metal-Organic Frameworks. *Angew. Chem. Int. Ed. Engl.* **2015**, *54*, 3417–3430.

(24) Taylor, J. M.; Dekura, S.; Ikeda, R.; Kitagawa, H. Defect Control To Enhance Proton Conductivity in a Metal–Organic Framework. *Chem. Mater.* **2015**, *27*, 2286–2289.

(25) Wu, H.; Chua, Y. S.; Krungleviciute, V.; Tyagi, M.; Chen, P.; Yildirim, T.; Zhou, W. Unusual and Highly Tunable Missing-Linker Defects in Zirconium Metal–Organic Framework UiO-66 and Their Important Effects on Gas Adsorption. *J. Am. Chem. Soc.* **2013**, *135*, 10525–10532.

(26) Cliffe, M. J.; Hill, J. A.; Murray, C. A.; Coudert, F.-X.; Goodwin, A. L. Defect-Dependent Colossal Negative Thermal Expansion in UiO-66(Hf) Metal–organic Framework. *Phys. Chem. Chem. Phys.* **2015**, *17*, 11586–11592.

(27) Chizallet, C.; Bats, N. External Surface of Zeolite Imidazolate Frameworks Viewed Ab Initio: Multifunctionality at the Organic−Inorganic Interface. *J. Phys. Chem. Lett.* **2010**, *1* (1), 349–353.

(28) Chizallet, C.; Lazare, S.; Bazer-Bachi, D.; Bonnier, F.; Lecocq, V.; Soyer, E.; Quoineaud, A.-A. A.; Bats, N. Catalysis of Transesterification by a Nonfunctionalized Metal-Organic Framework: Acido-Basicity at the External Surface of ZIF-8 Probed by FTIR and Ab Initio Calculations. TL - 132. *J. Am. Chem. Soc.* **2010**, *132*, 12365–12377.

(29) Canivet, J.; Fateeva, A.; Guo, Y.; Coasne, B.; Farrusseng, D. Water Adsorption in MOFs: Fundamentals and Applications. *Chem. Soc. Rev.* **2014**, *43*, 5594–5617.

(30) Burtch, N. C.; Jasuja, H.; Walton, K. S. Water Stability and Adsorption in Metal–Organic Frameworks. *Chem. Rev.* **2014**, *114*, 10575–10612.

(31) Liang, J.; Su, J.; Wang, Y.; Chen, Y.; Zou, X.; Liao, F.; Lin, J.; Sun, J. A 3D 12-Ring Zeolite with Ordered 4-Ring Vacancies Occupied by (H2O)2 Dimers. *Chemistry* **2014**, *20*, 16097–16101.

(32) Bai, Z.; Fujii, M.; Imakita, K.; Hayashi, S. Strong White Photoluminescence from Annealed Zeolites. *J. Lumin.* **2014**, *145*, 288–291.

(33) Baerlocher, C.; Xie, D.; McCusker, L. B.; Hwang, S.-J.; Chan, I. Y.; Ong, K.; Burton, A. W.; Zones, S. I. Ordered Silicon Vacancies in the Framework Structure of the Zeolite Catalyst SSZ-74. *Nat. Mater.* **2008**, *7*, 631–635.

(34) Yu, K.; Kiesling, K.; Schmidt, J. R. Trace Flue Gas Contaminants Poison Coordinatively

Unsaturated Metal–Organic Frameworks: Implications for CO 2 Adsorption and Separation. *J. Phys. Chem. C* **2012**, *116*, 20480–20488.

(35) Park, K. S.; Ni, Z.; Côté, A. P.; Choi, J. Y.; Huang, R.; Uribe-Romo, F. J.; Chae, H. K.; O'Keeffe, M.; Yaghi, O. M.; O'Keeffe, M.; et al. Exceptional Chemical and Thermal Stability of Zeolitic Imidazolate Frameworks. *Proc. Natl. Acad. Sci. U. S. A.* **2006**, *103*, 10186–10191.

(36) Fei, H.; Cahill, J. F.; Prather, K. A.; Cohen, S. M. Tandem Postsynthetic Metal Ion and Ligand Exchange in Zeolitic Imidazolate Frameworks. *Inorg. Chem.* **2013**, *52*, 4011–4016.

(37) Jian, M.; Liu, B.; Liu, R.; Qu, J.; Wang, H.; Zhang, X. Water-Based Synthesis of Zeolitic Imidazolate Framework-8 with High Morphology Level at Room Temperature. *RSC Adv.* **2015**, *5*, 48433–48441.

(38) Shah, M.; Kwon, H. T.; Tran, V.; Sachdeva, S.; Jeong, H.-K. One Step in Situ Synthesis of Supported Zeolitic Imidazolate Framework ZIF-8 Membranes: Role of Sodium Formate. *Microporous Mesoporous Mater.* **2013**, *165*, 63–69.

(39) Cravillon, J.; Nayuk, R.; Springer, S.; Feldhoff, A.; Huber, K.; Wiebcke, M. Controlling Zeolitic Imidazolate Framework Nano- and Microcrystal Formation: Insight into Crystal Growth by Time-Resolved In Situ Static Light Scattering. *Chem. Mater.* **2011**, *23*, 2130–2141.

(40) Phan, A.; Doonan, C. J.; Uribe-Romo, F. J.; Knobler, C. B.; O'Keeffe, M.; Yaghi, O. M. Synthesis, Structure, and Carbon Dioxide Capture Properties of Zeolitic Imidazolate Frameworks. *Acc. Chem. Res.* **2010**, *43*, 58–67.

(41) Deria, P.; Mondloch, J. E.; Karagiaridi, O.; Bury, W.; Hupp, J. T.; Farha, O. K. Beyond Post-Synthesis Modification: Evolution of Metal-Organic Frameworks via Building Block Replacement. *Chem. Soc. Rev.* **2014**, *43*, 5896–5912.

(42) Karagiaridi, O.; Lalonde, M. B.; Bury, W.; Sarjeant, A. A.; Farha, O. K.; Hupp, J. T. Opening ZIF-8: A Catalytically Active Zeolitic Imidazolate Framework of Sodalite Topology with Unsubstituted Linkers. *J. Am. Chem. Soc.* **2012**, *134*, 18790–18796.

(43) Wang, Z.; Cohen, S. M. Postsynthetic Modification of Metal-Organic Frameworks. *Chem. Soc. Rev.* **2009**, *38*, 1315–1329.

(44) Cheng, P.; Hu, Y. H. H 2 O-Functionalized Zeolitic Zn(2-Methylimidazole) 2 Framework (ZIF-8) for H 2 Storage. *J. Phys. Chem. C* **2014**, *118*, 21866–21872.

(45) Blöchl, P. E. Projector Augmented-Wave Method. *Phys. Rev. B* **1994**, *50*, 17953–17979.

(46) Kresse, G.; Furthmüller, J. Efficiency of Ab-Initio Total Energy Calculations for Metals and Semiconductors Using a Plane-Wave Basis Set. *Comput. Mater. Sci.* **1996**, *6*, 15–50.

(47) Kresse, G. Efficient Iterative Schemes for Ab Initio Total-Energy Calculations Using a Plane-Wave Basis Set. *Phys. Rev. B* **1996**, *54*, 11169–11186.

(48) Kresse, G.; Hafner, J. Ab Initio Molecular Dynamics for Liquid Metals. *Phys. Rev. B* **1993**, *47*, 558–561.

(49) Kresse, G.; Hafner, J. Ab Initio Molecular-Dynamics Simulation of the Liquid-Metal–amorphous-Semiconductor Transition in Germanium. *Phys. Rev. B* **1994**, *49*, 14251–14269.

(50) Kresse, G. From Ultrasoft Pseudopotentials to the Projector Augmented-Wave Method. *Phys. Rev. B* **1999**, *59*, 1758–1775.

(51) Henkelman, G.; Jónsson, H. Improved Tangent Estimate in the Nudged Elastic Band Method for Finding Minimum Energy Paths and Saddle Points. *J. Chem. Phys.* **2000**, *113*, 9978.

(52) Henkelman, G.; Uberuaga, B. P.; Jónsson, H. A Climbing Image Nudged Elastic Band Method for Finding Saddle Points and Minimum Energy Paths. *J. Chem. Phys.* **2000**, *113*, 9901.

(53) Marenich, A. V; Cramer, C. J.; Truhlar, D. G. Universal Solvation Model Based on Solute Electron Density and on a Continuum Model of the Solvent Defined by the Bulk Dielectric Constant and Atomic Surface Tensions. *J. Phys. Chem. B* **2009**, *113*, 6378–6396.